

High Harmonic Generation by Bright Squeezed Vacuum

Andrei Rasputnyi^{1,2}, Zhaopin Chen^{3,4,5}, Michael Birk^{3,4,5},
Oren Cohen^{3,4,5}, Ido Kaminer^{4,5,6}, Michael Krüger^{3,4,5},
Denis Seletskiy⁷, Maria Chekhova^{1,2,6*}, Francesco Tani^{1,8}

¹Max Planck Institute for the Science of Light, Staudtstr. 2, Erlangen, 91058, Germany.

²Friedrich-Alexander Universität Erlangen-Nürnberg, Staudtstr. 7/B2, Erlangen, 91058, Germany.

³Department of Physics, Technion – Israel Institute of Technology, Technion City, Haifa, 32000, Israel.

⁴Solid State Institute, Technion – Israel Institute of Technology, Technion City, Haifa, 32000, Israel.

⁵Helen Diller Quantum Center, Technion – Israel Institute of Technology, Technion City, Haifa, 32000, Israel.

⁶Faculty of Electrical and Computer Engineering, Technion – Israel Institute of Technology, Technion City, Haifa, 32000, Israel.

⁷femtoQ Laboratory, Department of Engineering Physics, Polytechnique Montréal, Montréal, Québec H3T 1J4, Canada.

⁸Univ. Lille, CNRS, UMR 8523—PhLAM—Physique des Lasers Atomes et Molécules, Lille, F-59000, France.

*Corresponding author(s). E-mail(s): maria.chekhova@mpl.mpg.de;

Abstract

We observe non-perturbative high harmonic generation in solids pumped by a macroscopic quantum state of light, bright squeezed vacuum (BSV), which we generate in a single spatiotemporal mode. Due to its broad photon-number distribution, covering states from **0** to **2 × 10¹³** photons per pulse, and sub-cycle electric field fluctuations over $\pm 1 \text{ V}/\text{\AA}$, BSV provides access to free carrier dynamics within a much broader range of peak intensities than accessible with coherent light. It is also considerably more efficient in the generation of high harmonics than coherent light of the same mean intensity.

1 Introduction

High harmonic generation (HHG) is an extreme nonlinear optical process resulting in the generation of coherent high-frequency radiation under intense laser illumination of matter, such as gases [1–4] and solids [5–7]. It enables the generation of attosecond light pulses [8, 9], giving access to a vast range of ultrafast phenomena at the natural time scale of electron motion. In contrast to conventional nonlinear optics, HHG involves complex electron dynamics, which is explained by a three-step mechanism [10–12]. Figure 1(b) depicts the mechanism in bulk solids: creation of an electron-hole pair through tunneling, its acceleration in the laser field (intraband HHG), and finally, electron-hole recombination, with the acquired kinetic energy released in the form of high-frequency photons (interband HHG). The control of electron dynamics at optical frequencies paves the way to petahertz electronics [13], outperforming current standards of data processing. HHG allows all-optical energy band structure retrieval [6], extreme ultraviolet spectroscopy [14], laser picoscopy of the valence electron structure [15], investigations of quantum phase transitions [16] and Berry phases [17], to name a few.

Although HHG essentially relies on the quantum properties of the matter, the intense light field driving it is usually considered to be classical (Fig. 1(a)). Hitherto, there have been no experiments employing quantum states of light for driving HHG. Meanwhile, recent works reveal quantum-optical features in the radiation of both high harmonics [18–20] and the driver as a result of generating them [21–23]. Still, all these works deal with the HHG from classical (coherent) pulses of light. The use of quantum light for pumping HHG has been considered theoretically [24, 25] but not realized up to now since HHG requires intensities on the order of 1 TW cm^{-2} , or photon numbers about 10^{13} at a timescale of tens of femtoseconds, which so far were inaccessible for quantum state engineering. Indeed, quantum states of light produced in quantum optics typically contain only a few photons per mode. A macroscopic quantum state can be obtained by adding a strong coherent component to a squeezed vacuum [26] or to a single photon [27, 28], but even in this case, most of the energy is contained in the classical part [29].

An exception is bright squeezed vacuum (BSV), a macroscopic quantum state of light generated at the output of a strongly pumped unseeded optical parametric amplifier. BSV is a quantum superposition of even-photon-number states, with the strongest contribution from the vacuum but with very high photon numbers contributing considerably. The mean photon number $\langle N \rangle$ of BSV achieved in recent experiments was as high as 10^{13} [30, 31], with the photon-number probability distribution so broad that photon numbers exceeding the mean by a factor of 6 or more occurred with 2 % probability. This feature is in striking contrast with the photon-number distribution of coherent (classical) light, whose width is as small as $\Delta N = \sqrt{\langle N \rangle}$ (the shot-noise

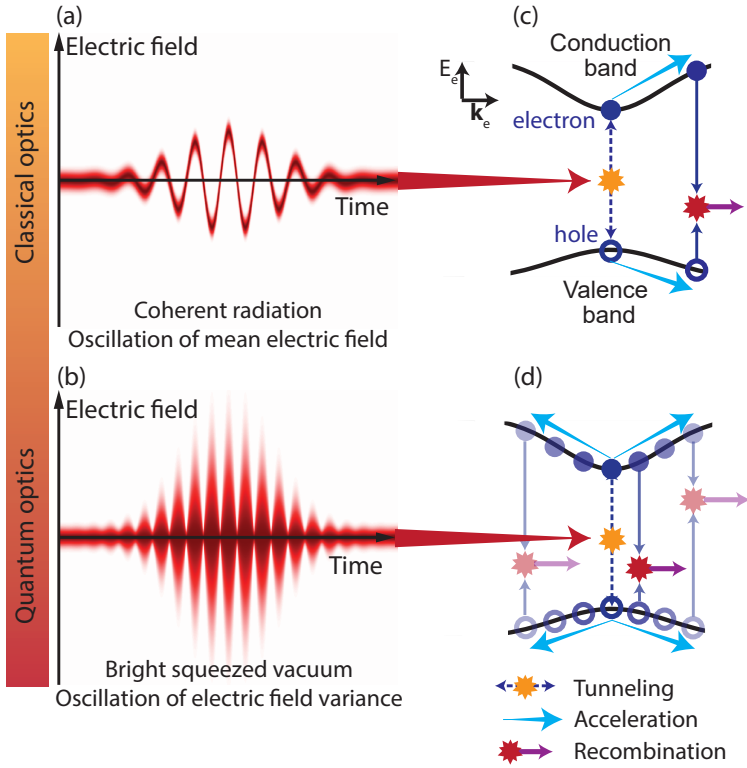


Fig. 1 (a) The electric field of a coherent pulse exhibits a mean value oscillating at the optical frequency and a constant variance. (b) The electric field of a bright squeezed vacuum pulse. Its mean value is zero at every time moment, while the variance oscillates at twice the carrier frequency. (c) High harmonic generation by coherent light in a semiconductor in the interband mechanism. An electron-hole pair emerges via perturbative (multiphoton) or non-perturbative excitation, is accelerated by the electric field, gaining energy, and finally recombines, emitting high-energy photons. (d) High harmonic generation by bright squeezed vacuum in a semiconductor. Due to the extremely noisy nature of the BSV field, the high harmonic generation is driven by a quantum state of light comprised of a wide range of photon numbers and an ambiguity in the sign of the electric field.

limit). For coherent light with $\langle N \rangle = 10^{13}$, events happening with 2% probability have photon numbers that differ from the mean by less than $10^{-4}\%$.

BSV has been shown to manifest non-classical features as sub-shot-noise photon-number correlations [32] and polarization entanglement [33]. It was also predicted to enhance sub-cycle sensing of quantum optical fields [34]. The broad photon-number probability distribution of BSV leads to superbunching [35]: its intensity correlation function of order n , $g^{(n)} \equiv \langle :N^2:\rangle/\langle N \rangle^2$, is considerably higher than for thermal light. This feature becomes more pronounced at large n : while for thermal light, the correlation functions are $g_{th}^{(n)} = n!$, for BSV they are $g_{BSV}^{(n)} = (2n-1)!!$. Superbunching enhances multiphoton effects like perturbative harmonic generation [30] or nonlinear electron emission from nanotips [36].

Recent theoretical works propose applications of BSV in strong-field physics, predicting an extended plateau for HHG [24], modification of electron dynamics [25, 37],

and quadrature squeezing in the extreme ultraviolet spectral range [38]. Motivated by these proposals, here we demonstrate the experimental observation of BSV-driven HHG in solid-state targets.

In contrast to a bright coherent pulse, which has a well-defined amplitude of the electric field with very weak fluctuations (Fig. 1(a)), the mean electric field of the BSV remains at zero for all times, while its variance oscillates at twice the light frequency (Figure 1(c)) [39, 40]. This feature indicates strong quantum fluctuations of the field on a sub-cycle timescale. Due to these fluctuations, a BSV pulse is capable of driving electrons in a solid not only with a certain quasi-momentum k at a time, as in the case of a coherent pulse (Fig. 1(b)), but within a broad range of quasi-momenta simultaneously (Fig. 1(d)), including oppositely directed. Accordingly, within half of the optical cycle the electron-hole pairs can be spread all over the energy bands, emitting a broad spectrum of harmonic radiation. It also means that multi-photon and tunneling mechanisms of HHG, corresponding to different field values, can be realized simultaneously.

2 Results

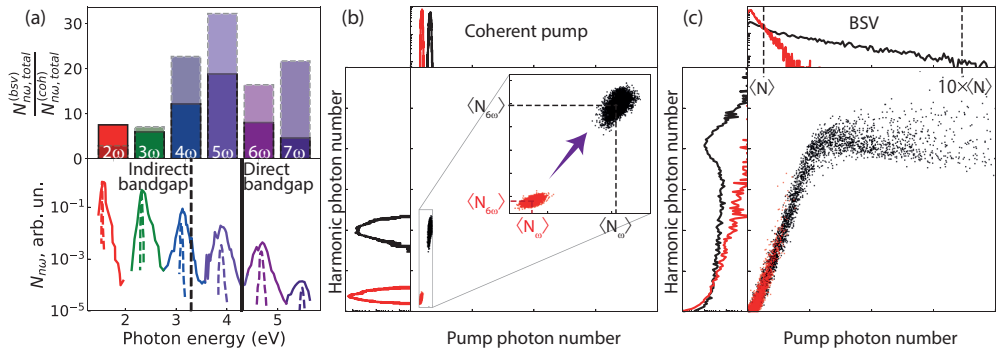


Fig. 2 (a) The spectrum of harmonics generated in a $6 \mu\text{m}$ x-cut doped lithium niobate crystal by bright squeezed vacuum (solid line) and by coherent radiation (dashed line). The photon energies of the 6th and the 7th harmonics exceed the direct energy bandgap of doped lithium niobate. Upper panel: Harmonic yield enhancement factor BSV vs. coherent pump for the same mean intensity ($\sim 2 \times 10^{13} \text{ W cm}^{-2}$). We show experimental (solid lines) and simulated (dashed) factors. (b),(c) Joint photon-number probability distribution of the input pump (b, coherent radiation, c, bright squeezed vacuum) and the 6th harmonic for two different mean pump photon numbers (red and black). In the case of coherent pump, the joint photon-number distribution is Gaussian while the photon statistics in the BSV case show non-trivial features.

In this work we report the first observation of HHG excited by quantum light. We compare HHG from solid targets driven by ultrashort pulses of coherent and quantum light. Both pulses are centred at $1.6 \mu\text{m}$ (0.77 eV), with the first having a duration of 70 fs at full-width half maximum (FWHM) and the latter of 25 fs (FWHM). We use two targets: $6 \mu\text{m}$ -thick x-cut Mg:LiNbO_3 (LN) and $1 \mu\text{m}$ -thick amorphous silicon (a-Si), observing emission of harmonics up to the 7th order.

The HHG spectrum of LN (Fig. 2(a)) shows both odd and even harmonics, due to the non-centrosymmetric crystal structure, while there are only odd harmonics from a-Si. The photon energies of the 2nd, the 3rd and the 4th harmonics from LN are below the indirect bandgap (3.3 eV [41]), the 5th harmonic photon energy is between the direct (4.3 eV [41]) and indirect bandgaps, and the 6th and 7th harmonics are above the direct bandgap (Fig. 2(a)). Despite the shorter duration, the BSV-generated 4th-7th harmonics show at least 5 to 15 times higher yield than the same harmonics driven by coherent pulses with identical mean intensity (2 TW cm⁻²).

Simulations based on the semiconductor-Bloch equations and accounting for the BSV photon statistics shows a similar behavior (see Fig. 2(a) and Methods).

Besides measuring the mean value of the harmonic yield, we also study the joint photon-number statistics between the input pump light and the harmonic radiation. For this purpose, we measure the shot-to-shot input light intensity and the resulting harmonic intensities (see Methods). Figures 2(b,c) show the measured two-dimensional photon-number distributions between the pump and the 6th harmonic from LN in the case of the coherent pump (panel b) and BSV pump (panel c) for two different mean photon numbers (red and black points). The photon-number probability distribution for coherent light is narrow and Gaussian, centered at the mean photon number $\langle N_\omega \rangle$. The photon-number probability distribution of the harmonic is also Gaussian with the mean photon number $\langle N_{6\omega} \rangle$ (Figure 2(b)). The increase of the pump's mean photon number shifts the center of the joint probability distribution without significantly changing its width. The measurement of the mean photon number is thus sufficient to find the harmonic yield $\langle N_{6\omega} \rangle / \langle N_\omega \rangle$, but obtaining the power scaling requires a systematic scan of the pump mean photon number.

In contrast to coherent radiation, BSV has a broad photon-number distribution with the maximum at zero photon number. The photon-number distribution of the harmonic inherits the large width of the driving pulse; moreover, there is a correlation between the BSV photon number and the harmonic photon number (Fig. 2(c)). As a result, the large variance of the BSV photon number reveals the entire power dependence through a single joint probability distribution measurement. In other words, a scan in the mean photon number of the BSV excitation is not required, underscored by the fact that both low and high BSV setting (red vs black in Figure 2(c)) can reveal the entire power dependence.

Figure 3 shows the (shot-to-shot) power scaling of the 5th and 7th harmonics from amorphous silicon generated by BSV (a,b) and coherent radiation (c,d). For coherent pumping, we observe non-perturbative power scaling for both the 5th and the 7th harmonics: $N_{5\omega} \propto N_\omega^{2.8}$, $N_{7\omega} \propto N_\omega^{2.7}$. These results point to the non-perturbative regime of the 5th and the 7th harmonic generation in a-Si. However, in the case of BSV the scaling is different. For the 5th harmonic, the scaling with the power is perturbative, $N_{5\omega} \propto N_\omega^5$, up to the saturation regime above ~ 2 TW cm⁻². This can be explained by the superbunched photon statistics of BSV, which leads to the enhancement of n -photon processes by a factor of $g_{BSV}^{(n)}$, compared to coherent light [30]. In the case of the 5th harmonic generation by BSV, the enhancement is $g_{BSV}^{(5)} = 945$. Although the 7th harmonic generated by BSV already shows the non-perturbative scaling as a sign of tunneling scenario, its exponent is larger than in case of coherent pump, which

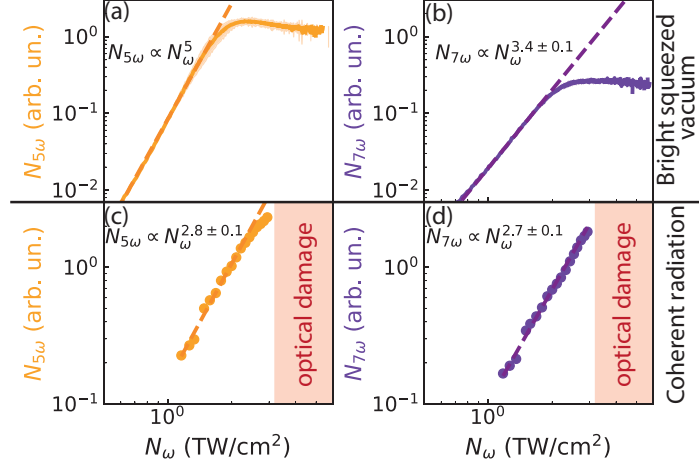


Fig. 3 Power scaling of the 5th and 7th harmonics generated in amorphous silicon by bright squeezed vacuum (a,b), and by coherent radiation (c,d) (solids lines: mean photon number of harmonic, shaded area: photon number variance of harmonic for particular input pump peal intensity). For coherent light excitation, the range above 2 TW/cm^2 is inaccessible because of sample damage.

points to a possible competition between the 7-photon multiphoton process and the non-perturbative regime of HHG. Another feature of harmonics generation by BSV is the saturation of the yield, which we attribute to the strong depletion of the valence band population. Remarkably, this is not observed in the case of coherent pump due to the optical damage of the sample.

For the x-cut magnesium-doped LN sample, the dependence of the harmonics power on the pump power is more complicated (Fig. 4) because this sample possesses much more complex free-carrier dynamics, non-centrosymmetric crystalline structure and doping. In the case of coherent pump, the below-bandgap harmonics show perturbative power scalings, starting to saturate below 1 TW cm^{-2} (Fig. 4(e,f)). The 6th and 7th harmonics demonstrate non-perturbative power scaling within the whole range of intensities (Fig. 4(g,h)).

Meanwhile, the 4th and 5th harmonics generated by BSV show perturbative power scaling for peak intensities up to 2 TW cm^{-2} , within a range broader than under pumping with coherent light. Similar to the a-Si case, this effect can be attributed to the multiphoton transitions enhanced due to the BSV superbunching. The 6th and 7th harmonics, which are above the direct bandgap, exhibit non-perturbative power scaling within the whole range of intensities, similar to the coherent case (Fig. 4(a-d)), with a higher exponent in the case of the 7th harmonic. This feature explains the lower statistical enhancement for these harmonics compared to the 5th harmonic (Fig. 2a). A power scaling with the exponent around 3 leads to the enhancement by only a factor of $g_{BSV}^{(3)} = 15$, instead of $g_{BSV}^{(5)} = 945$ in the case of the 5th harmonic. Above 1.5 TW cm^{-2} , the scaling exhibits two plateaus, especially pronounced for the 4th and 7th harmonics. These features are visible only in the case of the BSV pump, due to its possibility of ‘non-invasive’ testing. We attribute these features to the complex

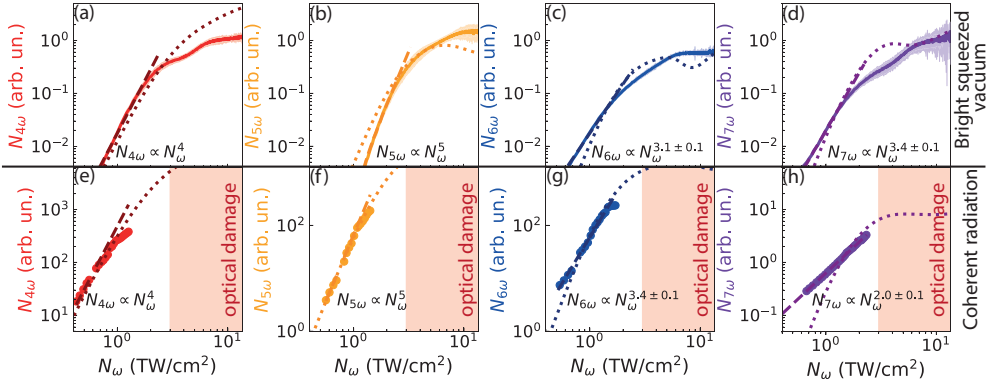


Fig. 4 Power scaling of the 4th-7th harmonics generated in x-cut lithium niobate by bright squeezed vacuum (a-d), and by coherent radiation (e-h) (solids lines: mean photon number of harmonic, shaded area: photon number variance of harmonic for particular input pump peak intensity). Dotted lines: numerical simulation. Dashed lines: power law fit. For coherent light excitation, the range above 3 TW cm^{-2} is inaccessible because of the sample damage.

structure of the sample. Numerical simulations can reproduce our experimental results fairly well both for coherent and BSV excitation (see Fig. 4 and Methods).

3 Discussion

The power scaling of harmonics from lithium niobate obtained with the coherent pump (Fig. 4(e-h)) terminates at around 2 TW cm^{-2} , which is close to the sample damage threshold. However, when pumping with BSV pulses, we can extend the range of peak intensities for harmonics generation. Figure 4(a-d) shows the harmonic power scaling reaching a peak intensity of 10 TW cm^{-2} , which is inaccessible with our coherent pump due to the instant damage of the sample. Under coherent-light irradiation, each pulse contains a definite amount of photons, which will cause the optical damage of the sample above a certain threshold. The BSV pump has a broad photon-number distribution, meaning that each pulse contains an uncertain number of photons, with the mean value far below the damage threshold. However, the large-photon-number events in the tail of the distribution can cause HHG and probe the material without damaging it in an instant or due to prolonged exposure. Furthermore, continuous irradiation of the sample within temporal intervals shorter than its relaxation time can result in optical damage to the sample. However, the BSV photon-number distribution also implies a longer temporal interval between intense events, thus effectively providing the sample with sufficient time to relax to its initial state. Thus, the excitation of a material with BSV is more gentle than with coherent light. It enables the study of solid-state samples in extreme regimes, such as the harmonic yield saturation in amorphous silicon (Fig. 3(a, b)), which can be related to the creation of an electron-hole plasma.

HHG driven by BSV can be used for quantum state engineering. By adjusting the input state of light, or selecting samples with proper band structure, free carriers will

recombine into particular quantum states of light. Figure 2(c) shows that the harmonic radiation has a non-trivial photon-number distribution.

BSV-driven HHG is also useful for spectroscopy. Within a single optical cycle of BSV, the superposition of photon-number states of BSV is mapped to the quasi-momentum of an electron; therefore, its wavefunction is distributed over the whole energy band. The joint photon-number distribution between the BSV and its harmonic, which results from the electron-hole recombination, contains the information about the band structure and electron dynamics inside the sample.

The harmonics power scaling obtained with BSV for lithium niobate (Fig. 4(a-d)) shows different features compared to silicon (Fig. 3(a,b)) which are attributed to solid state physics. On par with conventional frequency or time-domain spectroscopic approaches, photon-number statistics become a new spectroscopic knob, heralding the emergence of extreme nonlinear quantum spectroscopy.

4 Methods

4.1 Experimental setup

Figure 5(a) shows a sketch of our experimental setup for HHG in solids. For comparison, we use two linearly polarised pump sources delivering (i) coherent pulses and (ii) BSV pulses both centered at 1600 nm. As a pump laser for both sources, we use amplified titanium sapphire laser (Coherent Legend) with a central wavelength of 800 nm, 45 fs FWHM pulse duration, and repetition rate of 1 kHz. Combining this laser with a femtosecond OPA (Light Conversion, TOPAS Prime), we obtain coherent pulses with a duration of 70 fs (FWHM).

In a parallel setup, after reducing the pump laser beam size to 3 mm ($1/e^2$), we generate BSV in a 3-mm-thick BBO crystal cut for type-I collinear frequency-degenerate phase matching via high-gain parametric down-conversion. Here, the BBO crystal is tuned out of the exact phase matching to reduce the frequency bandwidth of the BSV, so that the BSV becomes single-mode temporally. However, at this stage, BSV pulses still contain around 150 spatial modes. In order to make it single-mode also spatially, we reflect both the BSV and the pump back into the same crystal with a plane silver mirror placed at a distance of 75 cm from the crystal. Back at the BBO, only the BSV spatial mode with the lowest diffraction (e.g, the fundamental mode) overlaps significantly with the pump beam and undergoes phase-sensitive amplification, while all the higher-order modes diffract faster without being further amplified [42]. After the amplification, the BSV pulses exhibit a spectral bandwidth of 150 nm centered around 1.6 μ m, and we separate them from the residual 800 nm light using a shortpass dichroic mirror (Thorlabs DMSP1180) and two longpass filters (Thorlabs FELH1000).

To characterize the temporal profile of the coherent and BSV pulses, and thus determine the actual intensity of the light irradiating the sample, we use a home-build device for second-harmonic frequency-resolved optical gating (SH-FROG). The retrieved FROG traces reveal that both pulses are almost transform-limited with a duration of 70 fs FWHM for the coherent pulses and 25 fs FWHM for the BSV pulses (the measured FROG trace of the latter ones is shown in 5(c)).

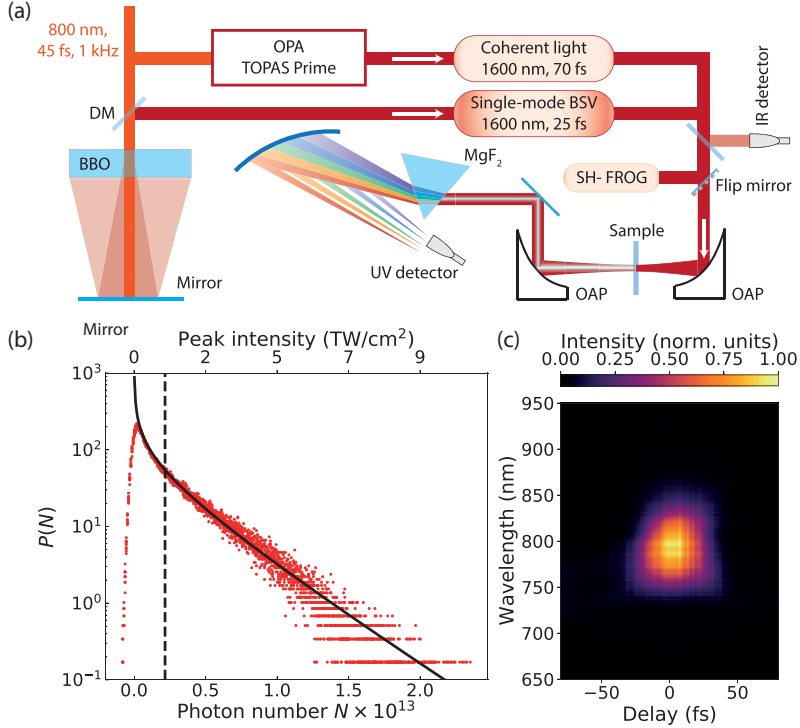


Fig. 5 (a) Experimental setup for HHG by coherent radiation and BSV. (b) Photon-number distribution of BSV. The solid line is a theoretical fit, which corresponds to single-mode BSV, the only fitting parameter being the mean photon number (dashed line). (c) Measured average FROG trace of BSV.

Figure 5(b) displays the photon-number distribution of BSV measured with a fast InGaAs photodiode (Thorlabs PDA20C2) without spatial or spectral filtering. The data are well fitted with a theoretical single-mode distribution [30] (black line), with the mean number of photons per pulse $2 \cdot 10^{12}$ (dashed vertical line), confirming that the BSV is single-mode. The distribution stretches up to photon numbers of $2 \cdot 10^{13}$, corresponding to pulse energies of $9 \mu\text{J}$.

For HHG, either the BSV or the coherent radiation is focused into a $30 \mu\text{m}$ spot (at $1/e^2$) on the sample with a silver off-axis parabolic mirror (Edmund Optics, $f = 25.4 \text{ mm}$) for driving HHG. The spot size has been determined from a knife-edge measurement for both sources. We use two samples: an x-cut $6 \mu\text{m}$ Mg:LiNbO₃ crystal on a 1 mm fused silica substrate and a $1 \mu\text{m}$ amorphous silicon layer on a 1 mm fused silica substrate. We mount the samples so that the substrate faces the pump pulses. Because fused silica possesses a significantly higher bandgap, it does not contribute to the outcome of the HHG measurement. Both the harmonics and the input light are collimated by a UV-enhanced aluminum off-axis parabolic mirror (Thorlabs MPD119-F01, $f = 25.4 \text{ mm}$) and sent to a MgF₂ prism. After this, the harmonics are focused by a UV-enhanced aluminum spherical mirror (Thorlabs CM254-250-F01) to different positions.

We detect the 4th–7th harmonics by a fast UV-enhanced silicon avalanche photodiode (Thorlabs APD440A2) separately by rotating the spherical mirror within a range of 1°. Additionally, we place bandpass filters for the 4th harmonic (Thorlabs FBH400-40), the 5th harmonic (Edmund Optics 12094, BP325/50) and the 6th harmonic (Edmund Optics 39313, BP266/10), and also an iris (1 mm opening) in front of the detector to reduce the contribution of scattered light. We acquire 200,000 single-shot records of input coherent light or BSV pulses and each harmonic synchronously.

4.2 Numerical simulation

To simulate and elucidate our experimental findings, we utilize the semiconductor-Bloch equations (SBEs) [43] to describe the interaction between BSV (or coherent) light and LiNbO_3 along Γ - Z :

$$\frac{\partial P(k, t)}{\partial t} = [\epsilon_c(k) - \epsilon_v(k) + iE(t)\nabla_k]P(k, t) - (1 - f_k^e - f_k^h)d_k \cdot E(t) - i\frac{1}{T_2}P(k, t), \quad (1)$$

$$\frac{\partial f_k^{e(h)}(k, t)}{\partial t} = -2\text{Im}[d_k \cdot E(t) \cdot P_k^*] + eE(t)\nabla_k f_k^{e(h)}(k, t). \quad (2)$$

Here, $P(k, t)$ represents a dimensionless polarization depending on the time t and the quasi-momentum k . $f_k^{e(h)}$ denotes the population of electrons and holes in the conduction and valence bands, respectively. The energy-momentum relation for the conduction band $\epsilon_c(k)$ and the valence band $\epsilon_v(k)$, as well as the transition dipole moment (TDM) d_k are derived from density functional theory (DFT) [44], with some modifications. Most importantly, we set the bandgap manually to 4.3 eV, corresponding to the direct bandgap most relevant for the HHG process.

To eliminate multiple recollision interferences and maintain the pronounced harmonic structure in our 1D simulation, we set the phenomenological decoherence time to half of the optical cycle duration of the pump laser, $T_2 = 0.5T_{\text{pump}}$. Extending the decoherence time to one optical cycle T_{pump} does not notably alter our results. In general, a longer decoherence time exceeding a few cycles allows electrons to return over longer durations than a laser cycle, leading to aperiodic photon emission, whereas a shorter decoherence time less than a quarter cycle $0.25T_{\text{pump}}$ may significantly suppress long trajectories.

Considering LiNbO_3 ’s ferroelectric nature, we account for the spontaneous polarization effect, which breaks the material’s symmetry and allow for even-order harmonics generation (see Ref. [44] for more details). The HHG spectrum is computed as follows:

$$S_{\text{HHG}}(\omega) \sim \left| \int_{-\infty}^{\infty} [J_{\text{inter}} + iJ_{\text{intra}}] e^{i\omega t} dt \right|^2, \quad (3)$$

where

$$J_{\text{inter}} = \frac{d}{dt} \int d_k \cdot P(k, t) dk + \text{c.c.}, \quad (4)$$

$$J_{\text{intra}} = \sum_{n=c,v} \int \nu_n(k) \cdot f_n(k, t) dk \quad (5)$$

where J_{inter} and J_{intra} denote the interband and intraband contributions to the HHG yield, and $\nu_n(k) = \nabla_k \epsilon_n(k)$ represents the group velocity of the electrons .

For simulating the BSV-pumped HHG spectrum underlying the enhancement plot (Fig. 2(a), we employ the Husimi Q function for BSV light [24]:

$$Q(\epsilon_\alpha) \approx \frac{2}{\sqrt{2\pi|\bar{\epsilon}|^2}} \exp\left(-\frac{|\epsilon_\alpha|^2}{2|\bar{\epsilon}|^2}\right). \quad (6)$$

Here, ϵ_α is the electric field amplitude with coherent parameter α , and $\bar{\epsilon}$ is mean value of absolute amplitude of the BSV field.

The BSV-pumped HHG spectrum is obtained by integrating the coherent HHG spectra with the Q function distribution [24]:

$$S_{\text{HHG}}^{\text{BSV}}(\omega, \bar{\epsilon}) = \int d\epsilon_\alpha Q(\epsilon_\alpha) S_{\text{HHG}}^{\text{coh}}(\omega, \epsilon_\alpha). \quad (7)$$

Acknowledgements. F.T., M.C. and A.R. thank Philip St.J. Russell for supporting the project. The authors thank Matan Even Tzur and Misha Ivanov for fruitful discussions. A.R. thanks Patrick Cusson for the help with the FROG measurement and Isaac Soward for the help at the first stage of the experiment. A.R. acknowledges funding from the International Max Planck Research School for Physics of Light. D.S. acknowledges partial support by the European Union’s Horizon Europe Research and Innovation Programme under agreement 101070700 (project MIRALQS). Z.C., M.B., O.C., I.K. and M.K. thank the Helen Diller Quantum Center for partial financial support.

Author contributions. M.C. and F.T. conceived the project, supervised the work and acquired the funding. A.R., F.T. and M.C. designed the experiment. A.R. carried out the experiment under supervision of M.C., F.T. and D.S. Z.C. and M.B. developed the theory and carried out the numerical simulations under the supervision of M.K., I.K. and O.C. A.R., M.C., D.S., M.K. and F.T. wrote the article. All authors contributed to discussions and the interpretation of the results.

References

- [1] Ferray, M., L’Huillier, A., Li, X.F., Lompre, L.A., Mainfray, G., Manus, C.: Multiple-harmonic conversion of 1064 nm radiation in rare gases. *J. Phys. B: At. Mol. Opt. Phys.* **21**(3), 31–35 (1988) <https://doi.org/10.1088/0953-4075/21/3/001>
- [2] McPherson, A., Gibson, G., Jara, H., Johann, U., Luk, T.S., McIntyre, I.A., Boyer, K., Rhodes, C.K.: Studies of multiphoton production of vacuum-ultraviolet radiation in the rare gases. *J. Opt. Soc. Am. B* **4**, 595–601 (1987) <https://doi.org/10.1364/JOSAB.4.000595>
- [3] Krausz, F., Ivanov, M.: Attosecond physics. *Rev. Mod. Phys.* **81**, 163–234 (2009) <https://doi.org/10.1103/RevModPhys.81.163>

- [4] Popmintchev, T., Chen, M.-C., Popmintchev, D., Arpin, P., Brown, S., Ališauskas, S., Andriukaitis, G., Balčiunas, T., Mücke, O.D., Pugzlys, A., Baltuška, A., Shim, B., Schrauth, S.E., Gaeta, A., Hernández-García, C., Plaja, L., Becker, A., Jaron-Becker, A., Murnane, M.M., Kapteyn, H.C.: Bright coherent ultrahigh harmonics in the kev x-ray regime from mid-infrared femtosecond lasers. *Science* **336**(6086), 1287–1291 (2012) <https://doi.org/10.1126/science.1218497>
- [5] Ghimire, S., DiChiara, A.D., Sistrunk, E., Agostini, P., DiMauro, L.F., Reis, D.A.: Observation of high-order harmonic generation in a bulk crystal. *Nature Physics* **7**, 138–141 (2011) <https://doi.org/10.1038/nphys1847>
- [6] Vampa, G., Hammond, T.J., Thiré, N., Schmidt, B.E., Légaré, F., McDonald, C.R., Brabec, T., Klug, D.D., Corkum, P.B.: All-optical reconstruction of crystal band structure. *Phys. Rev. Lett.* **115**, 193603 (2015) <https://doi.org/10.1103/PhysRevLett.115.193603>
- [7] Goulielmakis, E., Brabec, T.: High harmonic generation in condensed matter. *Nature Photonics* **16**(6), 411–421 (2022) <https://doi.org/10.1038/s41566-022-00988-y>
- [8] Hentschel, M., Kienberger, R., Spielmann, C., Reider, G.A., Brabec, T., Corkum, P., Heinzmann, U., Drescher, M., Krausz, F.: Attosecond metrology. *Nature* **414**, 509–513 (2001) <https://doi.org/10.1038/35107000>
- [9] Paul, P.M., Toma, E.S., Breger, P., Mullot, G., Augé, F., Balcou, P., Muller, H.G., Agostini, P.: Observation of a train of attosecond pulses from high harmonic generation. *Science* **292**(5522), 1689–1692 (2001) <https://doi.org/10.1126/science.1059413>
- [10] Corkum, P.B.: Plasma perspective on strong field multiphoton ionization. *Phys. Rev. Lett.* **71**(13), 1994–1997 (1993) <https://doi.org/10.1103/PhysRevLett.71.1994>
- [11] Lewenstein, M., Balcou, P., Ivanov, M.Y., L’Huillier, A., Corkum, P.B.: Theory of high-harmonic generation by low-frequency laser fields. *Phys. Rev. A* **49**, 2117–2132 (1994) <https://doi.org/10.1103/PhysRevA.49.2117>
- [12] Vampa, G., Hammond, T.J., Thiré, N., Schmidt, B.E., Légaré, F., McDonald, C.R., Brabec, T., Corkum, P.B.: Linking high harmonics from gases and solids. *Nature* **522**, 462–464 (2015) <https://doi.org/10.1038/nature14517>
- [13] Borsch, M., Meierhofer, M., Huber, R., Kira, M.: Lightwave electronics in condensed matter. *Nature Reviews Materials* **8**(10), 668–687 (2023) <https://doi.org/10.1038/s41578-023-00592-8>
- [14] Luu, T.T., Garg, M., Kruchinin, S.Y., Moulet, A., Hassan, M.T., Goulielmakis, E.: Extreme ultraviolet high-harmonic spectroscopy of solids. *Nature* **521**(7553),

498–502 (2015) <https://doi.org/10.1038/nature14456>

- [15] Lakhotia, H., Kim, H.Y., Zhan, M., Hu, S., Meng, S., Goulielmakis, E.: Laser picoscopy of valence electrons in solids. *Nature* **583**, 55–59 (2020) <https://doi.org/10.1038/s41586-020-2429-z>
- [16] Alcalà, J., Bhattacharya, U., Biegert, J., Ciappina, M., Elu, U., Graß, T., Grochowski, P.T., Lewenstein, M., Palau, A., Sidiropoulos, T.P.H., Steinle, T., Tyulnev, I.: High-harmonic spectroscopy of quantum phase transitions in a high- T_c superconductor. *Proceedings of the National Academy of Sciences* **119**(40), 2207766119 (2022) <https://doi.org/10.1073/pnas.2207766119>
- [17] Uzan-Narovlansky, A.J., Faeyrman, L., Brown, G.G., Shames, S., Narovlansky, V., Xiao, J., Arusi-Parpar, T., Kneller, O., Bruner, B.D., Smirnova, O., Silva, R.E.F., Yan, B., Jiménez-Galán, Ivanov, M., Dudovich, N.: Observation of interband berry phase in laser-driven crystals. *Nature* **626**, 66–71 (2024) <https://doi.org/10.1038/s41586-023-06828-5>
- [18] Gorlach, A., Neufeld, O., Rivera, N., Cohen, O., Kaminer, I.: The quantum-optical nature of high harmonic generation. *Nature Communications* **11**(1), 4598 (2020) <https://doi.org/10.1038/s41467-020-18218-w>
- [19] Sloan, J., Gorlach, A., Tzur, M.E., Rivera, N., Cohen, O., Kaminer, I., Soljačić, M.: Entangling extreme ultraviolet photons through strong field pair generation (2023). <https://doi.org/10.48550/arXiv.2309.16466>
- [20] Yi, S., Babushkin, I., Smirnova, O., Ivanov, M.: Generation of massively entangled bright states of light during harmonic generation in resonant media (2024). <https://doi.org/10.48550/arXiv.2401.02817>
- [21] Tsatrafyllis, N., Kominis, I.K., Gonoskov, I.A., Tzallas, P.: High-order harmonics measured by the photon statistics of the infrared driving-field exiting the atomic medium. *Nature Communications* **8**(1), 15170 (2017) <https://doi.org/10.1038/ncomms15170>
- [22] Tsatrafyllis, N., Kühn, S., Dumergue, M., Foldi, P., Kahaly, S., Cormier, E., Gonoskov, I.A., Kiss, B., Varju, K., Varro, S., Tzallas, P.: Quantum optical signatures in a strong laser pulse after interaction with semiconductors. *Phys. Rev. Lett.* **122**, 193602 (2019) <https://doi.org/10.1103/PhysRevLett.122.193602>
- [23] Lewenstein, M., Ciappina, M.F., Pisanty, E., Rivera-Dean, J., Stammer, P., Lamprou, T., Tzallas, P.: Generation of optical schrödinger cat states in intense laser–matter interactions. *Nature Physics* **17**(10), 1104–1108 (2021) <https://doi.org/10.1038/s41567-021-01317-w>
- [24] Gorlach, A., Tzur, M.E., Birk, M., Krüger, M., Rivera, N., Cohen, O., Kaminer, I.: High-harmonic generation driven by quantum light. *Nature Physics* **19**(11),

1689–1696 (2023) <https://doi.org/10.1038/s41567-023-02127-y>

[25] Even Tzur, M., Birk, M., Goralch, A., Krüger, M., Kaminer, I., Cohen, O.: Photon-statistics force in ultrafast electron dynamics. *Nature Photonics* **17**(6), 501–509 (2023) <https://doi.org/10.1038/s41566-023-01209-w>

[26] Vahlbruch, H., Mehmet, M., Danzmann, K., Schnabel, R.: Detection of 15 db squeezed states of light and their application for the absolute calibration of photoelectric quantum efficiency. *Phys. Rev. Lett.* **117**, 110801 (2016) <https://doi.org/10.1103/PhysRevLett.117.110801>

[27] Bruno, N., Martin, A., Sekatski, P., Sangouard, N., Thew, R.T., Gisin, N.: Displacement of entanglement back and forth between the micro and macro domains. *Nature Physics* **9**(9), 545–548 (2013) <https://doi.org/10.1038/nphys2681>

[28] Lvovsky, A.I., Ghobadi, R., Chandra, A., Prasad, A.S., Simon, C.: Observation of micro–macro entanglement of light. *Nature Physics* **9**(9), 541–544 (2013) <https://doi.org/10.1038/nphys2682>

[29] Laghaout, A., Neergaard-Nielsen, J.S., Andersen, U.L.: Assessments of macroscopicity for quantum optical states. *Optics Communications* **337**, 96–101 (2015) <https://doi.org/10.1016/j.optcom.2014.07.046>. Macroscopic quantumness: theory and applications in optical sciences

[30] Spasibko, K.Y., Kopylov, D.A., Krutyanskiy, V.L., Murzina, T.V., Leuchs, G., Chekhova, M.V.: Multiphoton effects enhanced due to ultrafast photon-number fluctuations. *Phys. Rev. Lett.* **119**, 223603 (2017) <https://doi.org/10.1103/PhysRevLett.119.223603>

[31] Manceau, M., Spasibko, K.Y., Leuchs, G., Filip, R., Chekhova, M.V.: Indefinite-mean pareto photon distribution from amplified quantum noise. *Phys. Rev. Lett.* **123**, 123606 (2019) <https://doi.org/10.1103/PhysRevLett.123.123606>

[32] Finger, M.A., Iskhakov, T.S., Joly, N.Y., Chekhova, M.V., Russell, P.S.J.: Raman-free, noble-gas-filled photonic-crystal fiber source for ultrafast, very bright twin-beam squeezed vacuum. *Phys. Rev. Lett.* **115**, 143602 (2015) <https://doi.org/10.1103/PhysRevLett.115.143602>

[33] Iskhakov, T.S., Agafonov, I.N., Chekhova, M.V., Leuchs, G.: Polarization-entangled light pulses of 10^5 photons. *Phys. Rev. Lett.* **109**, 150502 (2012) <https://doi.org/10.1103/PhysRevLett.109.150502>

[34] Virally, S., Cusson, P., Seletskiy, D.V.: Enhanced electro-optic sampling with quantum probes. *Phys. Rev. Lett.* **127**, 270504 (2021) <https://doi.org/10.1103/PhysRevLett.127.270504>

- [35] Iskhakov, T.S., Pérez, A.M., Spasibko, K.Y., Chekhova, M.V., Leuchs, G.: Super-bunched bright squeezed vacuum state. *Opt. Lett.* **37**(11), 1919–1921 (2012) <https://doi.org/10.1364/OL.37.001919>
- [36] Heimerl, J., Mikhaylov, A., Meier, S., Höllerer, H., Kaminer, I., Chekhova, M., Hommelhoff, P.: Multi-photon electron emission with non-classical light (2023). <https://doi.org/10.48550/arXiv.2307.14153>
- [37] Even Tzur, M., Cohen, O.: Motion of charged particles in bright squeezed vacuum. *Light: Science & Applications* **13**(1), 41 (2024) <https://doi.org/10.1038/s41377-024-01381-w>
- [38] Tzur, M.E., Birk, M., Gorlach, A., Kaminer, I., Krüger, M., Cohen, O.: Generation of squeezed high-order harmonics (2023). <https://doi.org/10.48550/arXiv.2311.11257>
- [39] Riek, C., Seletskiy, D.V., Moskalenko, A.S., Schmidt, J.F., Krauspe, P., Eckart, S., Eggert, S., Burkard, G., Leitenstorfer, A.: Direct sampling of electric-field vacuum fluctuations. *Science* **350**(6259), 420–423 (2015) <https://doi.org/10.1126/science.aac9788>
- [40] Riek, C., Sulzer, P., Seeger, M., Moskalenko, A.S., Burkard, G., Seletskiy, D.V., Leitenstorfer, A.: Subcycle quantum electrodynamics. *Nature* **541**(7637), 376–379 (2017) <https://doi.org/10.1038/nature21024>
- [41] Kase, S., Ohi, K.: Optical absorption and interband faraday rotation in litao₃ and linbo₃. *Ferroelectrics* **8**(1), 419–420 (1974) <https://doi.org/10.1080/00150197408234114>
- [42] Pérez, A.M., Iskhakov, T.S., Sharapova, P., Lemieux, S., Tikhonova, O.V., Chekhova, M.V., Leuchs, G.: Bright squeezed-vacuum source with 1.1 spatial mode. *Opt. Lett.* **39**(8), 2403–2406 (2014) <https://doi.org/10.1364/OL.39.002403>
- [43] Luu, T.T., Wörner, H.J.: High-order harmonic generation in solids: A unifying approach. *Phys. Rev. B* **94**, 115164 (2016) <https://doi.org/10.1103/PhysRevB.94.115164>
- [44] Shao, T.-J., Hu, F., Chen, H.-B.: Spontaneous polarization effects on solid high harmonic generation in ferroelectric lithium niobate crystals. *J. Phys. B: At. Mol. Opt. Phys.* **54**(24) (2021) <https://doi.org/10.1088/1361-6455/ac43f5>